V. Citro, P. Luchini, F. Giannetti, F. Auteri
Boundary-Layer Flows Past an Hemispherical Roughness Element: Dns, Global Stability and Sensitivity Analysis
Procedia IUTAM, Vol. 14, 2015, p. 173-181
doi:10.1016/j.piutam.2015.03.038

Available online at www.sciencedirect.com

ScienceDirect

Procedia IUTAM 14 (2015) 173 – 181

Procedia IUTAM

www.elsevier.com/locate/procedia

IUTAM_ABCM Symposium on Laminar Turbulent Transition

Boundary-layer flows past an hemispherical roughness element: DNS, global stability and sensitivity analysis

V. Citro[a,*], P.Luchini[a], F.Giannetti[a], F.Auteri[b]

[a] *DIIN, Universitá degli Studi di Salerno, Via Giovanni Paolo II 132, 84084 Salerno, Italy*
[b] *Dipartimento di Scienze e Tecnologie Aerospaziali, Politecnico di Milano, via La Masa 34, 20156 Milano, Italy*

Abstract

We investigate the full three-dimensional instability mechanism arising in the wake of an hemispherical roughness element immersed in a laminar Blasius boundary layer. The inherent three-dimensional flow pattern beyond the critical Reynolds number is characterized by coherent vortical structures called hairpin vortices. Direct numerical simulation is used to analyze the formation and the shedding of hairpin packets inside the shear layer. The first bifurcation characteristics are investigated by global stability tools. We show the spatial structure of the linear direct and adjoint global eigenmodes of the linearized Navier-Stokes operator and use structural sensitivity analysis to locate the region where the instability mechanism acts. Results show that the "wavemaker" driving the self-sustained instability is located in the region immediately past the roughness element, in the shear layer separating the outer flow from the wake region.

Selection and peer-review under responsibility of ABCM (Brazilian Society of Mechanical Sciences and Engineering)

Keywords: Roughness Element, TriGlobal Linear Stability, Hairpin vortices

1. Introduction

The effect of surface roughness on the transition of boundary layers from laminar to turbulent flow is an important topic in fluid mechanics which has received and still receives remarkable attention. In particular, transition on surfaces with large roughness protrusion height appears to be characterized by physical mechanisms that are different from those acting for lower roughness protrusion height and have yet not been clarified. The presence of small roughness elements at the wall produces small flow disturbances which linearly amplify while being transported downstream, eventually attaining the amplitude necessary to cause transition at a relatively large distance from the roughness elements that gave rise to them. Such disturbances are of two general types: Tollmien-Schlichting waves, well visible in experiments characterized by a two-dimensional roughness distribution [2], or longitudinal vortices inducing a transient growth of streamwise streaks of alternating high- and low-momentum fluid, which may grow enough to cause transition before having the possibility to decay [3]. Recent experiments [1] have also highlighted the possibility that properly shaped roughness may delay transition.

* Corresponding author.
E-mail address: vcitro@unisa.it

Selection and peer-review under responsibility of ABCM (Brazilian Society of Mechanical Sciences and Engineering)
doi:10.1016/j.piutam.2015.03.038

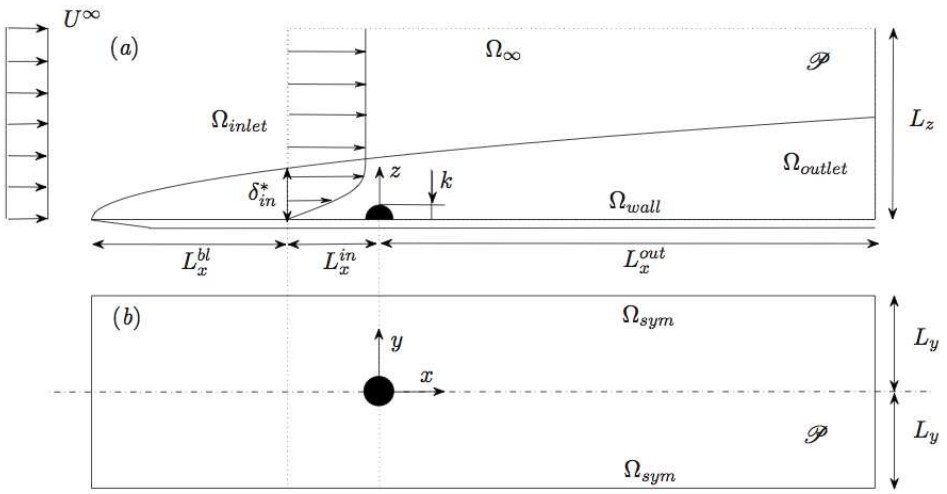

Fig. 1. Flow configuration, frame of reference and computational domain $\mathscr{P}$ (not in scale) are depicted using: (*a*) side view and (*b*) top view. The computational domain $\mathscr{P}$, delimited in the figures by a dotted line, extends from $x = -L_x^{in}$ to $x = L_x^{out}$ in the streamwise direction, from $z = 0$ to $z = L_z$ in the wall-normal direction and from $(-L_y \le y \le L_y)$ in the spanwise direction.

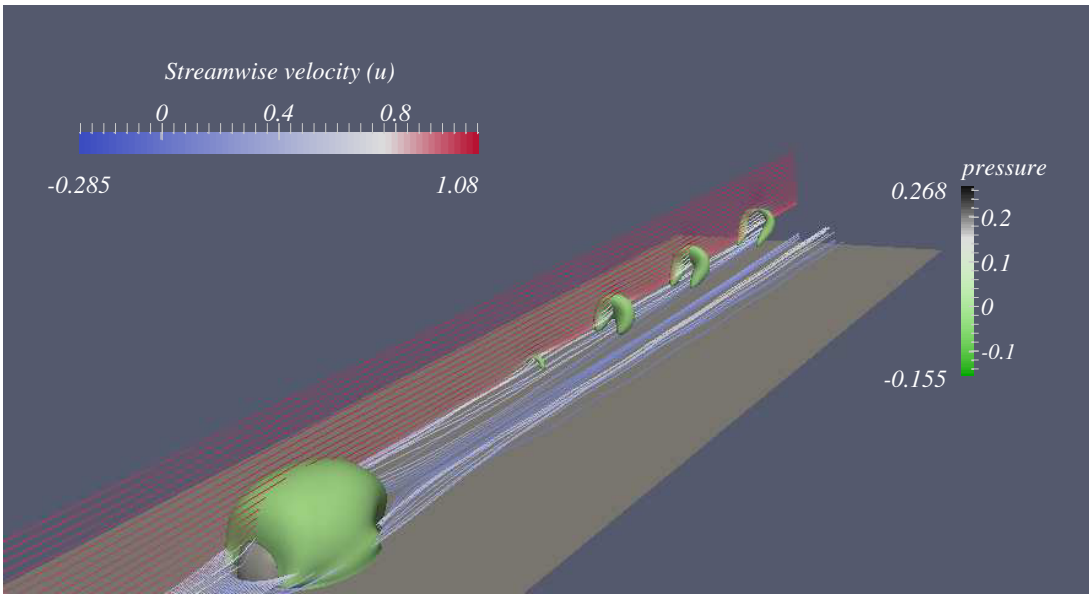

Fig. 2. Perspective view of the unsteady supercritical flow at $Re_k = 450$ and $k/\delta_k^* = 2.62$. Upstream velocity streamlines show the structure of the base flow near the hemispherical roughness element. The structure of hairpin vortices is depicted using iso-contour of pressure field. See Tab. 1 for further details of simulation parameters.

The transition scenario described above, however, only applies if the roughness amplitude is sufficiently small. On the other hand, when the protrusion height is large enough, transition suddenly appears downstream of an individual roughness element. The mechanism involved in this process is not yet understood. In an effort to shed light on the transition mechanism associated with large-amplitude surface roughness, several experiments have been carried out in the past (see *e.g.* Downs et al.[6] or Ergin et al.[4]). The results obtained have shown that if the Reynolds number based on the roughness height exceeds a critical value, then transition occurs immediately past the roughness element;

conversely, if the critical value is not exceeded, the scenario based on the transient grow mechanism mentioned above is dominant and transition takes place farther downstream. These experimental data as far back as in the '50s produced empirical correlations based on the roughness-based Reynolds number. These criterions are still used in practice to predict transition in the wake of isolated three-dimensional roughness elements. Although transition correlations are useful from a practical viewpoint, they are not able to reveal the detailed mechanism of transition, nor do they assist in designing transition control strategies besides simply placing design limits on acceptable roughness levels.

The aim of the present work is to provide an evidence that the transition process past a roughness element can be linked to a global (self-sustained) instability mechanism.

2. Problem formulation

We investigate the stability features of an incompressible Blasius boundary layer flow past an hemispherical obstacle. To ease comparisons with experimental investigations made by Klebanoff et al.[8], we have chosen to adopt a similar geometrical configuration.

In particular, we compare the critical Reynolds number with the one obtained by experiments in[8,10] and by direct numerical simulations in[9,7]. The problem is formulated in a standard cartesian coordinate system (x, y, z), whose origin is taken at the centre of the hemisphere as shown in Figure 1.

The fluid motion obeys the unsteady Navier-Stokes equations that read

$$\mathscr{M}\{\boldsymbol{U}\} = 0, \tag{1a}$$

$$\frac{\partial \boldsymbol{U}}{\partial t} + \mathscr{C}(\boldsymbol{U})\{\boldsymbol{U}\} = -\mathscr{G}P + \frac{1}{Re}\mathscr{D}\{\boldsymbol{U}\} \tag{1b}$$

where $P \in \mathbb{R}$ is the reduced pressure scalar field and $\boldsymbol{U} \in \mathbb{R}^3$ is the velocity vector with components $\boldsymbol{U} = (U, V, W)$. The gradient and divergence operators acting on the velocity field are given by $\mathscr{G} = \nabla \in \mathbb{R}^{3\times1}$ and by $\mathscr{M} = \nabla\cdot \in \mathbb{R}^{1\times3}$ respectively. Convective and diffusive operators, instead, are defined as $\mathscr{C}(\boldsymbol{U})\{\boldsymbol{U}\} = (\boldsymbol{U}\cdot\nabla)\boldsymbol{U} \in \mathbb{R}^{3\times3}$ and $\mathscr{D}\{\boldsymbol{U}\} = \nabla^2\boldsymbol{U} \in \mathbb{R}^{3\times3}$.

Equations (1) are made dimensionless using the total heigth k of the roughness element as the characteristic length scale and the velocity U_k of the incoming uniform stream that would exist in the boundary layer at the height k without roughness[8]. The Reynolds number is thus defined as $Re_k = U_k k/\nu$, with ν the fluid kinematic viscosity.

Experimental data[5] and numerical simulations[7] have shown that the topology of the flow around an isolated three-dimensional roughness element in a boundary layer consists of a steady horseshoe vortex that wraps around its upstream side and trails two steady counter-rotating leg vortices downstream. At sufficiently high values of the Reynolds number, unsteady hairpin vortices originate periodically from the separated region just behind the roughness element (see figure 1). The observation of vortex shedding in the wake of moderate-to-large-height elements supports the idea that transition beyond the critical Reynolds number is related to a global instability of the wake flow past the roughness element.

3. Numerical method

We use the spectral element method (SEM) implemented in Nek5000 to solve the governing equations (1). Thus, the unknowns $(\boldsymbol{U}, P)$ are spatially discretized onto $P_N - P_{N-2}$ spectral elements using Lagrange orthogonal polynomials on Gauss-Lobatto-Legendre (GLL) nodes. The temporal discretization of the momentum equations has been achieved using a semi-implicit splitting scheme. For further details, we refer to Tufo & Fischer[11].

The system of differential equations (1) is closed using no-slip boundary conditions at the roughness surface and at the flat plate (Ω_{wall}), standard outflow conditions at the outlet (Ω_{outlet}) and a fully developed Blasius profile, characterized by a variable boundary layer thickness δ^*_{in}, at the inlet (Ω_{inlet}). Finally, we adopt symmetry boundary conditions[9] at the upper side of the computational domain (Ω_∞) and at the lateral boundaries (Ω_{sym}).

A steady base-flow field cannot be reached simply using DNS when the Reynolds number exceeds its critical value. In order to obtain a steady base flow on which perform a stability analysis we implemented in Nek5000 a novel

stabilizing procedure called "boostconv". Such procedure is similar to a GMRES but with a continuous update of the Krylov subspace. The stabilized solution at a given time step is obtained by correcting the Nek5000 solution with a linear combination of the residuals at the previous time steps. The procedure has been implemented inside Nek5000 in a way to maintain the scalability of the code on heavily parallel machines. This new stabilization procedure works well to track both steady and unsteady bifurcations. An example of its use can be found in Carini et al.[12].

The eigenvalues and eigenmodes of the linearized (direct and adjoint) Navier-Stokes operator characterize the long-time dynamics of the perturbation field. In this context we look for solution of the linearized equations in the form $\{\mathbf{u}, p\}(x, y, z, t) = \{\hat{\mathbf{u}}, \hat{p}\}(x, y, z)\exp(\gamma t)$, where the real part of the complex eigenvalue $\gamma = \sigma \pm i\omega$ represents the temporal growth rate of the disturbance, while its imaginary part is the eigenfrequency of the direct $\{\hat{\mathbf{u}}, \hat{p}\}$ global mode. A similar decomposition is used to calculate the adjoint $\{\hat{\mathbf{u}}^\dagger, \hat{p}^\dagger\}$ global mode. All the eigenproblems involved in this work are solved by the Implicitly Restarted Arnoldi Method implemented in ParPACK[13] using the linearized (direct and adjoint) time-stepper available in Nek5000 code (see Bagheri[14] for further details).

The physical domain is decomposed in multi-block spectral sub-elements and the several grids are build symmetric with respect to the y-axis. In order to ensure that the spatial resolution is sufficient, several numerical convergence tests has been carried out. The convergence and the validation of the present numerical approach is reported in table 1.

We compare the results obtained using two computational domains: the first one is characterized by $L_x^{in} = 7R, L_x^{out} = 30R, L_y = 10R, L_z = 8R$ (this domain will be referred to as $\mathbb{M}1$), while the second (larger) domain is given by $L_x^{in} = 9R, L_x^{out} = 40R, L_y = 12R, L_z = 10R$ (named $\mathbb{M}2$). Here R represents the radius of the hemisphere. The mesh $\mathbb{M}1$ is discretized in space on a total of 8971 spectral elements having a polynomial expansion of $10 \times 10 \times 10$; $\mathbb{M}2$, instead, has 16987 elements with the same polynomial order. The choice of this polynomial basis involves 1000 points per element for a 3D case that leads to 8′971′000 total points for $\mathbb{M}1$ and 16′987′000 total points for $\mathbb{M}2$. In both cases we cluster the elements both in the wall-normal direction near the wall and along the plate near the roughness element. From table 1, it is clear that the domain $\mathbb{M}1$ is sufficient for accurately evaluating the most unstable eigenvalue growth rates, eigenfrequencies and the Strouhal number extracted from DNS.

Table 1. Convergence results. We show the effect of the size of the computational domain on the complex eigenvalue γ and on the Strouhal number extracted from DNS at the supercritical Reynolds number $Re_k = 450$ with $k/\delta_k^* = 2.62$ and compare our results with those obtained by Tufo *et al.*[9]. The Strouhal number (for DNS) reported here is obtained directly from a probe located in $(x, y, z) = (5R, R, R)$, i.e. in the region past the roughness element. (S. Direct=Global Stability analysis for direct eigenproblem, S. Adjoint=Global Stability analysis for adjoint eigenproblem)

	$\mathbb{M}1$		$\mathbb{M}2$		err(%)
Type	σ	$St = \frac{\omega k}{2\pi U_k}$	σ	$St = \frac{\omega k}{2\pi U_k}$	$\frac{\lvert\gamma_{\mathbb{M}1}\rvert - \lvert\gamma_{\mathbb{M}2}\rvert}{\lvert\gamma_{\mathbb{M}2}\rvert}$
S. Direct	$+8.7148 \times 10^{-2}$	0.1659	$+8.3329 \times 10^{-2}$	0.1653	1.23%
S. Adjoint	$+8.7148 \times 10^{-2}$	0.1659	$+8.3329 \times 10^{-2}$	0.1653	1.23%
DNS	(*unstable*)	0.1685	(*unstable*)	0.1684	–
Tufo *et al.*[9]	(*unstable*)	≈ 0.168	(*unstable*)	≈ 0.168	–

4. Results

In this work, we have performed a set of 3D direct numerical simulations to compute the flow characteristics for the case $k/\delta_k^* = 2.62$ at different Reynolds numbers. We chose this value of k/δ_k^* and the (hemispherical) shape of the roughness element to have a direct and easy comparison with the experimental results provided by Klebanoff et al.[8]. The unsteady equations have been advanced in time until either a steady flow or a periodic flow was obtained. As the Reynolds number is increased, we observe the occurrence of a limit cycle characterized by the periodic shedding of hairpin packets inside the boundary layer. The flow becomes unsteady for values of the Reynolds number around $Re_k \approx 450$. At this value the flow is already periodic and figure 1 shows a snapshot of the computed supercritical field. The simulation was advanced in time until a perfectly periodic flow was obtained. We use iso-contours of the pressure field to visualize hairpin vortices and velocity streamlines to show the distribution of the velocity near the hemisphere and in the wake region. In table 1 we show the main frequencies corresponding to the shedding of these hairpin packets obtained from the power spectrum analysis of the instantaneous data sampled at $(x, y, z) = (5R, R, R)$. This

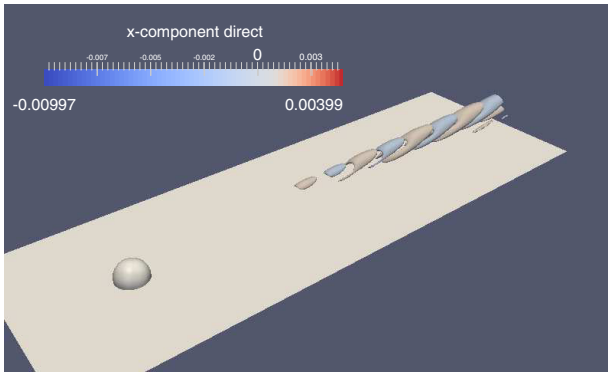

(a) Streamwise component.

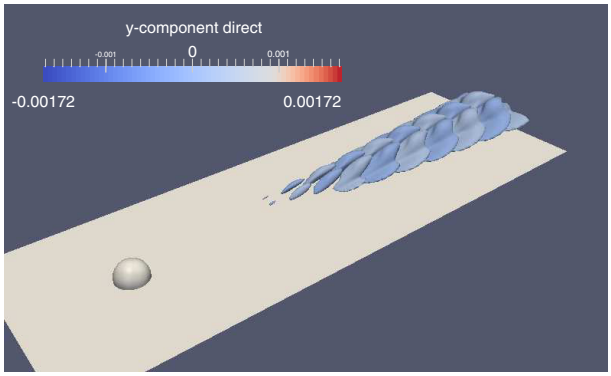

(b) Wall-normal component

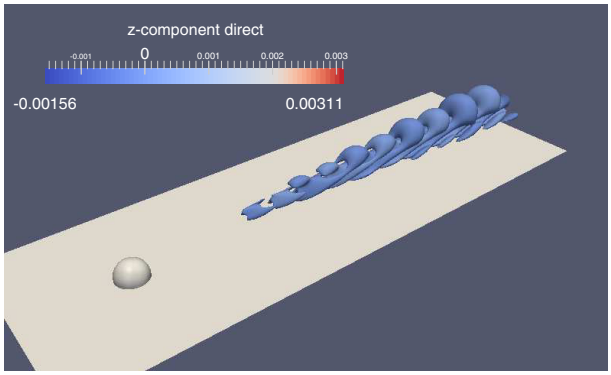

(c) Spanwise component

Fig. 3. Contour plot of the real part of the most unstable direct eigenmode for $Re_k = 450$, $k/\delta_k^* = 2.62$.

laminar periodic symmetric vortex shedding has been observed also in experiments by Acarlar & Smith[10], Klebanoff et al.[8] and in numerical simulations by Tufo et al.[9]. Such flow behavior suggests a possible link with the existence of a global instability that drives the flow to a limit cycle. To corroborate this hypothesis, we perform a TriGlobal stability analysis on top of the stabilized steady base flow at $Re_k = 450$. This was calculated using the previously mentioned stabilizing procedure "boostconv". The eigenvalue problems were solved by using the ParPACK which was coupled with the solvers of the linearized direct and adjoint Navier-Stokes equations present in Nek5000. The computed leading direct global mode is depicted in figure 3.

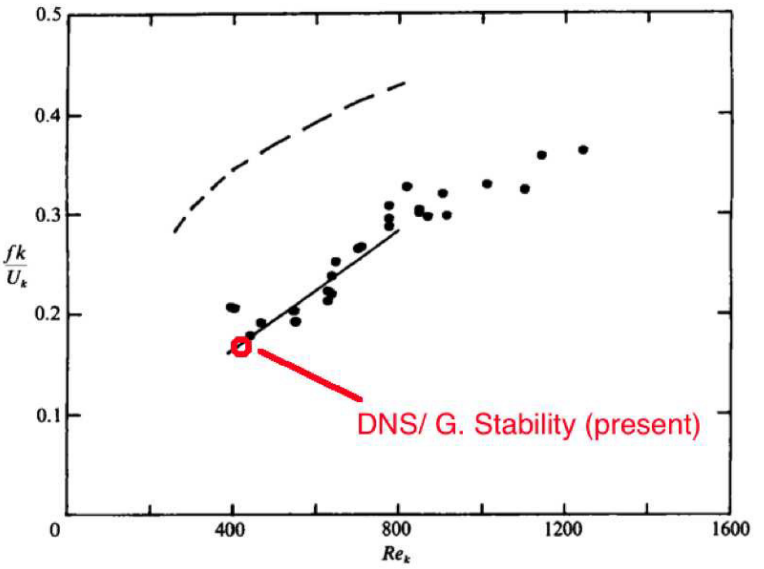

Fig. 4. Comparison of Strouhal behavior from experimental data by Klebanoff et al.[8]. The red circle indicates the critical frequency value obtained in the present numerical simulation.

The maximum of both streamwise, wall-normal and spanwise components is found downstream of the roughness element, almost at the end of the computational domain. To precisely locate where the perturbation reaches its maximum amplitude additional simulations have to be performed on longer domains. In fact, as for the cylinder case, the global mode increases exponentially in the streamwise direction, reaches its maximum and then slowly decays. However, even if a short domain was used for the present study, the computed eigenvalues are accurate since, as we will discuss, the instability mechanism is strongly localized behind the roughness element (see Giannetti & Luchini[15] for further details). Convergence tests performed on this configuration corroborate our statement. The frequency of the leading eigenmode is found to agree very well with DNS data (see table 1).

Moreover the critical Reynolds number determined by the stability analysis compares well with the transition threshold determined in the experiments. As an example, figure 4 shows the experimental data by Klebanoff et al.[8] and the critical data obtained in the present study.

In addition to the direct calculations, we also computed the adjoint eigenmode (see Schmid & Henningson[3] and Luchini & Bottaro[16] for further details) of the linearized Navier-Stokes operator. As we can observe in figure 5, the adjoint mode is spatially separated from the direct one, a feature which is due to the strong non-normality of the linearized Navier-Stokes operator. The different components of the adjoint mode reach their maximum magnitude close to the roughness element. The adjoint field gives interesting information on the receptivity of the mode to both initial conditions and to momentum forcing. Results show that the most receptive regions are those surrounding the hemisphere. In order to locate the instability mechanism we finally performed a structural sensitivity analysis as explained in[15]. In particular, in figure 6a, we show iso-surfaces of the spectral norm of the sensitivity tensor

$$\mathbf{S}(x,y,z) = \frac{\hat{\mathbf{u}}^{\dagger}(x,y,z)\,\hat{\mathbf{u}}(x,y,z)}{\int_{\mathcal{P}} \hat{\mathbf{u}}^{\dagger}(x,y,z)\cdot\hat{\mathbf{u}}(x,y,z)dV} \tag{2}$$

(where $\hat{\mathbf{u}}$ and $\hat{\mathbf{u}}^{\dagger}$ are respectively the velocity components of both the direct and the adjoint mode). As can be noted, the structural sensitivity is highly localized in a region just behind the roughness element, across the surface separating the outer flow from the wake region. This can be more easily observed in figure 6b where a contour plot on the symmetry plane is shown. The fact that the instability mechanism ("the wavemaker") is localized in a region of strong shear suggests that the instability could be related to a feedback mechanism involving Kelvin-Helmoltz waves. Parametric computations for different values of k/δ_k^* and a WKBJ analysis of this configuration are in progress and results will be reported in future publications.

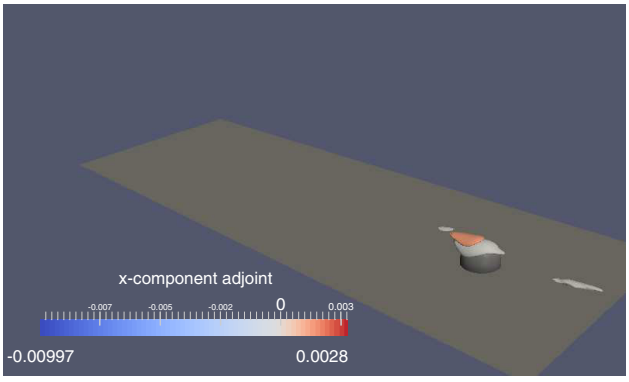

(a) Streamwise component.

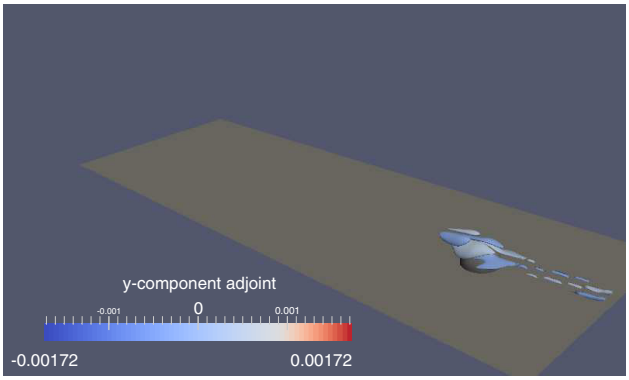

(b) Wall-normal component

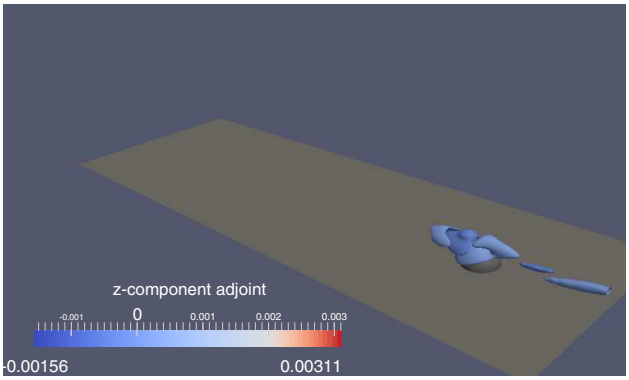

(c) Spanwise component

Fig. 5. Contour plot of the real part of the most unstable adjoint eigenmode for $Re_k = 450$, $k/\delta_k^* = 2.62$.

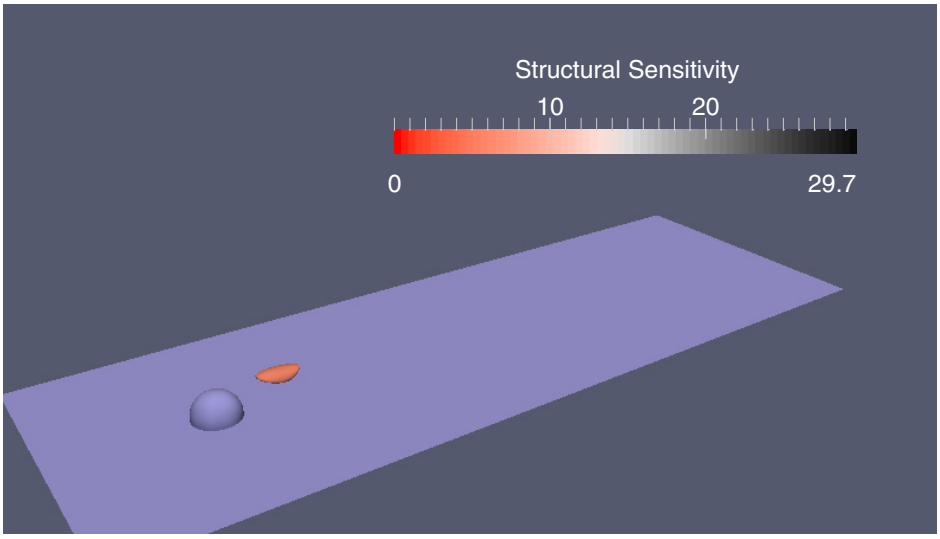

(a) Contour plot of the Structural sensitivity map.

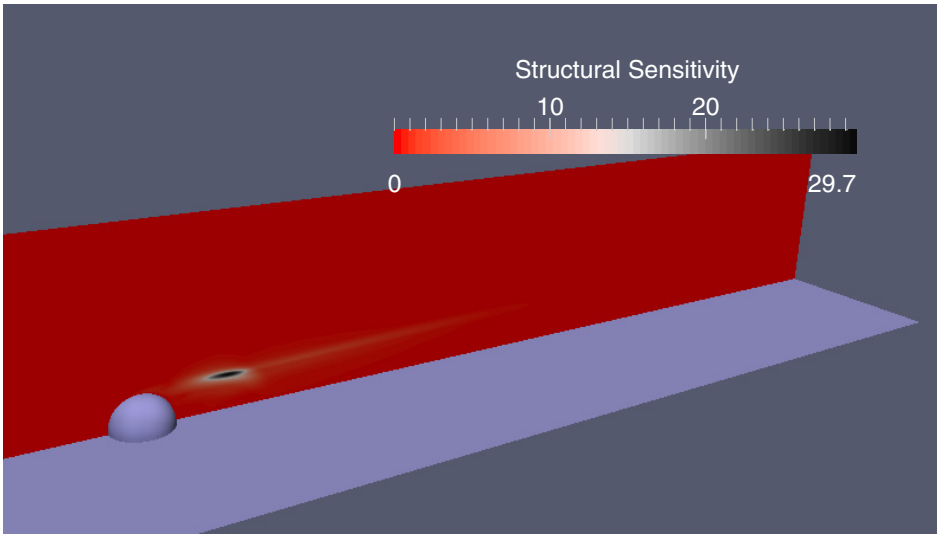

(b) Contour plot of the Structural sensitivity field on the plane $y = 0$.

Fig. 6. The structural sensitivity field has been calculated for $Re_k = 450$, $k/\delta_k^* = 2.62$.

5. Conclusions

The analysis presented in this work confirms the existence of a self-sustained mode in the wake of a hemispherical roughness element of large protrusion height invested by a Blasius boundary layer. Direct numerical simulations, stability and sensitivity analyses were performed to better understand the characteristics of the resulting flow. Results are in agreement with previous experimental data and show that when the Reynolds number is increased beyond a critical value the flow undergoes an Hopf bifurcation. The self-sustained mode giving rise to the periodic shedding of hairpin vortices has been found by computing a global stability analysis. The spatial characteristics of both direct and adjoint mode have been analyzed and the instability mechanism localized by using a structural sensitivity analysis. Results show that the instability mechanism is highly localized in the shear layer separating the outer flow region from the wake region.

Acknowledgements

Work supported by CINECA (PRACE), by European Commission through the FP7 project "RECEPT" (grant agreement no. ACPO-GA-2010-265094) and by the Regione Lombardia award under the LISA initiative, for the availability of high performance computing resources and support.

References

1. Fransson J. H. M., Brandt L., Talamelli A., Cossu C. Experimental and theoretical investigation of the non-modal growth of steady streaks in a flat plate boundary layer. *Phys. Fluids* 2004;**16**:3627. (doi: http://dx.doi.org/10.1063/1.1773493)
2. Saric W. D., Reed H.L., Kerschen E. J. Boundary-layer receptivity to freestream disturbances. *Annu. Rev. Fluid Mech.* 2002;**34**:291-319. (doi: http://dx.doi.org/10.1146/annurev.fluid.34.082701.161921)
3. Schmid P. J., Henningson D.S. Stability and transition in shear flows. Springer; 2001.
4. Ergin F. G., White E. B. Unsteady and transitional flows behind roughness elements *AIAA J.* 2006;**44**:2504-2514. (doi: http://dx.doi.org/10.2514/1.17459)
5. Denissen A., White E. B. Rougness-Induced Bypass Transition, Revisited *AIAA J.* 2008;**46**:1874-1877. (doi: http://dx.doi.org/10.2514/1.17459)
6. Downs S. D., White E. B., Denissen N. A. Transient Growth and Transition Induced by Random Distributed Roughness *AIAA J.* 2008;**46**:451-462. (doi: http://dx.doi.org/10.2514/1.31696)
7. Rizzetta D. P., Visbal M. R. Direct numerical simulations of flow past an array of distributed roughness elements *AIAA J.* 2007;**45**:1967-1976. (doi: http://dx.doi.org/10.2514/1.31696)
8. Klebanoff P. S., Cleveland W. G., Tidstrom K. D. On the evolution of a turbulent boundary layer induced by a three-dimensional roughness element *J. Fluid Mech.* 1992;**237**:101-187. (doi: http://dx.doi.org/10.1017/S0022112092003379)
9. Tufo H. M., Fischer P. F., Papka M. E., Blom K. Numerical Simulation and Immersive Visualization of Hairpin Vortices Proceedings of the *ACM/IEEE SC99 Conference on High Performance Networking and Computing*, IEEE Computer Society, 1999.
10. Acarlar M. S., Smith C. R. A study of hairpin vortices in a laminar boundary layer. Part 1. Hairpin vortices generated by a hemisphere protuberance *J. Fluid Mech.* 1987;**175**:1-41. (doi: http://dx.doi.org/10.1017/S0022112087000272)
11. Tufo H. M., Fischer P. F. Terascale spectral element algorithms and implementations *In Proceedings of the 1999 ACM/IEEE Conference on Supercomputing* 1999; ACM.
12. Carini M., Giannetti F., Auteri F. On the origin of the flip-flop instability of two side-by-side cylinder wakes *J. Fluid Mech.* 2014;**742**:552-576.
13. Lehoucq R. B., Sorensen D. C., Yang C. ARPACK Users' Guide *Journal Society for Industrial and Applied Mathematics* 1998.
14. Bagheri S. Computational Hydrodynamic Stability and Flow Control Based on Spectral Analysis of Linear Operators *Arch. Comput. Methods Eng.* 2011. (doi: http://dx.doi.org/10.1007/s11831-012-9074-0)
15. Giannetti F., Luchini P. Structural sensitivity of the first instability of the cylinder wake *Journal of Fluid Mechanics* 2007;**581**;167- 197
16. Luchini P., Bottaro A. Adjoint Equations in Stability Analysis *Annual Review of Fluid Mechanics* 2014;**46**;493-517